Peer Reviewed Paper openaccess

Spectral similarity algorithm-based image classification for oil spill mapping of hyperspectral datasets

Deepthi* and Tessamma Thomas

Department of Electronics, Cochin University of Science and Technology, Kochi, Kerala, India 682022

Contacts
dilishdeepthi@gmail.com

In remote sensing, the compositional information of part of the earth's surface is statistically evaluated by comparing known field or library spectra with the unknown image spectra, known as spectral matching or spectral similarity analysis. In this research, hybrid spectral similarity algorithms developed based on chi-square distance (CHI or χ^2) are used to retrieve useful information from the Hyperion hyperspectral oil spill image covering the area near Liaodong Bay of the Bohai Sea, China. In order to evaluate the discriminability of spectral similarity algorithms, a pixel-level matching is carried out between the reference vectors, viz. Oil Slick (O), Sheen (H), Sea Water (S) and Ship Track (T), collected visually from known areas in the image. The hybrid spectral similarity algorithms are statistically assessed for their performance using the spectral discriminatory measures (i) relative spectral discriminatory power (RSDPW), (ii) relative spectral discriminatory probability (RSDPB) and (iii) relative spectral discriminatory entropy (RSDE). Additionally, the selected hybrid algorithms are used on the Hyperion image subset to perform a pixel-based classification. Classification results revealed that the CHI-based hybrid algorithms performed better than all other hybrid spectral similarity methods. Therefore, the CHI-based hybrid algorithms demonstrated their superior spectral discrimination capacity to classify marine spectral classes for oil spill mapping from the hyperspectral dataset.

Keywords: chi-square distance, hybrid spectral similarity measures, hyperspectral image, oil spill, overall accuracy, spectral discriminatory measures

Introduction

Oil spills occur in the seas mainly due to transportation accidents, the release of oil by shipping operators and various production platforms.[1] The oil floats on the sea surface, causing severe damage to the marine ecosystem.[2] Real-time mapping and evaluation of oil spillage is critical in making quick decisions and to prevent severe after-effects.[3] As the marine environment is a very complex organic system, spectral changes occurring on the leaked oils can be measured only by a spectrally broad sensor.[4] Hyperspectral sensors are a type of imaging spectroscopy sensor that sample the reflective portion of the electromagnetic (EM) spectrum.

Correspondence
Deepthi (dilishdeepthi@gmail.com)

Received: 27 August 2020
Revised: 13 October 2020
Accepted: 14 October 2020
Publication: 28 October 2020
doi: 10.1255/jsi.2020.a14
ISSN: 2040-4565

Citation
Deepthi and T. Thomas, "Spectral similarity algorithm-based image classification for oil spill mapping of hyperspectral datasets", *J. Spectral Imaging* **9,** a14 (2020). https://doi.org/10.1255/jsi.2020.a14

This ranges from the visible (400–700 nm) to the near infrared (NIR) region (about 2400 nm), with hundreds of narrow contiguous bands of 10 nm width.[5,6] As hyperspectral sensors bring in exact details from the most significant part of the EM spectrum, many studies have been conducted based on their spectral properties. As has been reported previously,[3,6] hyperspectral techniques are very useful for distinguishing the presence of oil film on water surfaces[7] in the regions 440–900 nm[8] and 600–900 nm.[9] Later, numerous studies evaluated the extraction capability of hyperspectral sensors on light diesel and crude oil,[10,11] on ice-infested waters[12] and other different types of marine oil spill[13–15] more specifically in the visible-near infrared (VNIR) region.[16] Various spectral classification algorithms[17,18] and endmember extraction methodologies[19,20] have been developed to detect and monitor oil pollution, where reference selection for oil spill formed a critical topic of hyperspectral research.[21] The reference spectra are obtained either from the laboratory or field measurements, or from the remotely sensed image.[22–25] A field survey validating the remote sensing data for oil spills from the marine environment is not practical because of accessibility concerns and the complexity of the scene;[26] generally, the references are directly interpreted by photo-interpretation of remotely sensed images.[27]

The possibility of hyperspectral classification and target detection is extended with the development of spectral matching or similarity methods that measure the similarity between spectral signatures or reflectance curves.[28,29] But these individual spectral similarity algorithms have their own limitations in using the band-level information and for the degree of effectiveness in detecting oils from hyperspectral images.[30] Conversely, to negate the shortcomings of individual similarity measures like City Block Distance (CBD),[31] Spectral Angle Mapper (SAM),[32] Euclidean Distance (EUD),[33] Spectral Correlation Mapper (SCM),[34] Spectral Information Divergence (SID)[35] and Jeffries–Matusita Distance (JMD),[36] as well as to integrate their benefits, mixed or hybrid approaches are developed. Such methods clearly outperformed the individual components, as they combine the potentials of the individual measures.[37] Techniques such as feature enhanced spectral similarity[38] and hybrid similarity approaches, EUD-SAM, EUD-SCM,[33,39] SID-SAM,[40] SID-SCM,[41] JMD-SAM,[42] JMD-SCM[43] and CBD-SAM, CBD-SCM, JMD-CBD, JMD-EUD, SID-CBD, SID-EUD[44] have been evaluated on oil-affected hyperspectral imagery to produce a significant improvement over the individual spectral matching algorithms. The need for high-performing algorithms is always a challenge in remote sensing, mostly due to the day to day advances in sensor and related technologies.

Here, with this research, an attempt is made to scrutinise the classification performances of the chi-square distance (CHI)-based hybrid similarity measures for hyperspectral oil spill mapping as CHI statistics find the relationship between two variables by identifying very minute dissimilarities between the pixel vectors.[45,46] In this step, the newly developed CHI-based hybrid similarity algorithms, namely CHI-SAM, CHI-SCM, JMD-CHI and SID-CHI, are compared with other existing hybrid measures, namely CBD-SAM, CBD-SCM, EUD-SAM, EUD-SCM, JMD-CBD, JMD-EUD, JMD-SAM, JMD-SCM, SID-CBD, SID-EUD, SID-SAM and SID-SCM, to discriminate oil and the other related spectral classes. Furthermore, the performance is analysed with the help of discriminatory statistics, RSDPW, RSDPB and RSDE.[43,47,48] RSDPW is formulated to compare the effectiveness of two similarity measures, and RSDPB identifies a pixel vector of interest from an existing database or spectral library. The RSDE or Entropy is derived from RSDPB that measures the uncertainty of a similarity algorithm in material identification from a spectral library. Based on the discriminatory statistics, eight highly performing hybrid similarity algorithms, viz. SID-CHI, CHI-SCM, SID-CBD, SID-SCM, JMD-CHI, CHI-SAM, SID-EUD and SID-SAM, are selected. It is then implemented on the four marine spectral classes of the Hyperion image, viz. Oil Slick (364 samples), Sheen (959 samples), Sea Water (545 samples) and Ship Track (106 samples), revealing higher accuracies for the developed CHI-based hybrid similarity, namely CHI-SAM, CHI-SCM, JMD-CHI and SID-CHI, relative to the other non-CHI algorithms.

Materials and methods

Data description

This research uses the hyperspectral image data acquired by the United States' EO-1 Hyperion Earth observation satellite. The L1T level image (terrain-corrected and georeferenced based on ground control points) in GeoTiff format[49] of the crude oil accident, Serial ID: EO1H1200312007126110KZ (https://earthexplorer.usgs.gov), obtained by the satellite at 10:27 am (local time) on 6 May 2007, mostly covering the area near Liaodong Bay of the Bohai Sea, was studied and is shown in Figure 1. Hyperion has 242 contiguous spectral bands of wavelength range 400–2500 nm with a spatial resolution of 30 m/pixel and an average spectral resolution of 10 nm/band. The predicted signal-to-noise ratio (SNR) of this dataset performs well in VNIR bands, where the SNR can be up to 150. For short-wave infrared (SWIR) bands in the dataset, the SNR is around 50.[50,51]

Additionally, for wavelengths above 1900 nm, the SNR is even less than 50.[52] Generally, the effective wavebands in the Hyperion image for crude oil detection are in the VNIR region.[16] In the pre-processing stage after bad-band removal, 43 continuous bands ranging from bands 13 to 55 (central wavelength 477.6900–905.0500 nm) in the VNIR region are selected and processed for further studies on oil spill detection.

Workflow

Figure 2 shows the flow chart of the methodology adopted in this research. The Hyperion image is initially pre-processed using the spectral subset technique, and the bad bands are eliminated, leaving 43 bands for subsequent analysis in a subscene of 173 × 301 pixels. Further, the image is atmospherically corrected using Fast Line-of-Sight Atmospheric Analysis of Spectral Hypercubes (FLAASH) (https://www.harrisgeospatial.com/docs/FLAASH.html), which removes the effect of atmospheric scattering and absorption features,[53] generating the resultant reflectance image. FLAASH has an advantage of spectral polishing that removes consistent artefacts from an atmospherically corrected hyperspectral image. Spectral polishing is an inbuilt process that can be selected in the FLAASH.[54] Initially, the average[44] of each of the four classes, namely Oil Slick, Sheen, Sea Water and Ship Track, are collected from the known areas[52,55] using visual image interpretation to create the respective reference vector.[22,56] Oil Slick generally represents a thick layer with a definitive brown or black colour. Contrarily, sheens are the thin layer of oils or the least contaminated seawater around the true colour oil slicks, and are really difficult to distinguish.[6] Second, the similarity matching measure and spectral discriminatory algorithms are executed on these average reference vectors to select the best performing hybrid similarity measures. Finally, the unknown image spectra, namely Oil Slick (364 samples, Sheen (959 samples), Sea Water (545 samples) and Ship Track (106 samples) are compared with the reference vectors and examined using a confusion matrix.

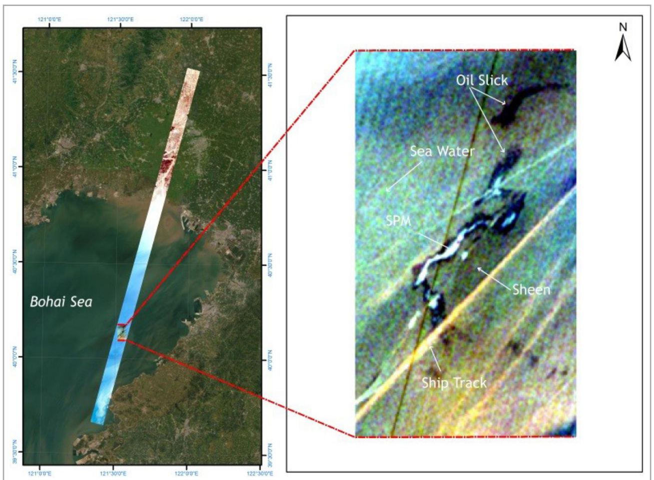

Figure 1. Remotely sensed Hyperion data coverage in the Bohai Sea (left); the typical targets are shown in the subset (right) (Red = Band 29, Green = Band 20, Blue = Band 13). The suspended particulate matter (SPM) aggregate, as seen in white, is not considered as a typical target as it has the same spectra of the Ship Track.

From Figure 3, it is evident that the spectral reflectance of water in the Ship Track is higher than that of the background Sea Water, which in turn is higher than the spectral reflectance of the Sheen and Oil Slick. As the thickness of the oil spill changes, the reflectance varies within the visible and NIR spectral ranges.[16] The suspended particulate matter (SPM) in the ship track formed by the movement of the ship leads to a rise in the water spectrum's reflective peak.[55,57] Also, as the sheen is translucent and contains very few hydrocarbons, the spectra of sheen are greatly influenced by sea water.[6] On the whole, all the classes follow nearly the same spectral curve. Therefore, a precise discrimination procedure is essential to differentiate between them. In this work, the formulation of a suitable procedure is addressed where the respective reference vector is made with the average reflectance values of each class.

To describe the pixel variability, similarity and discrimination in a Hyperion image, an information-theoretic spectral measure called Spectral Information Measure (SIM) is applied.[58] SIM models the spectral band-to-band inconsistency arising from uncertainty caused by randomness using four statistical moments, specifically the mean, variance, skewness (third central moment) and kurtosis (fourth central moment). SIM treats each pixel as a random variable utilising its spectral signature histogram as the desired probability distribution. By this

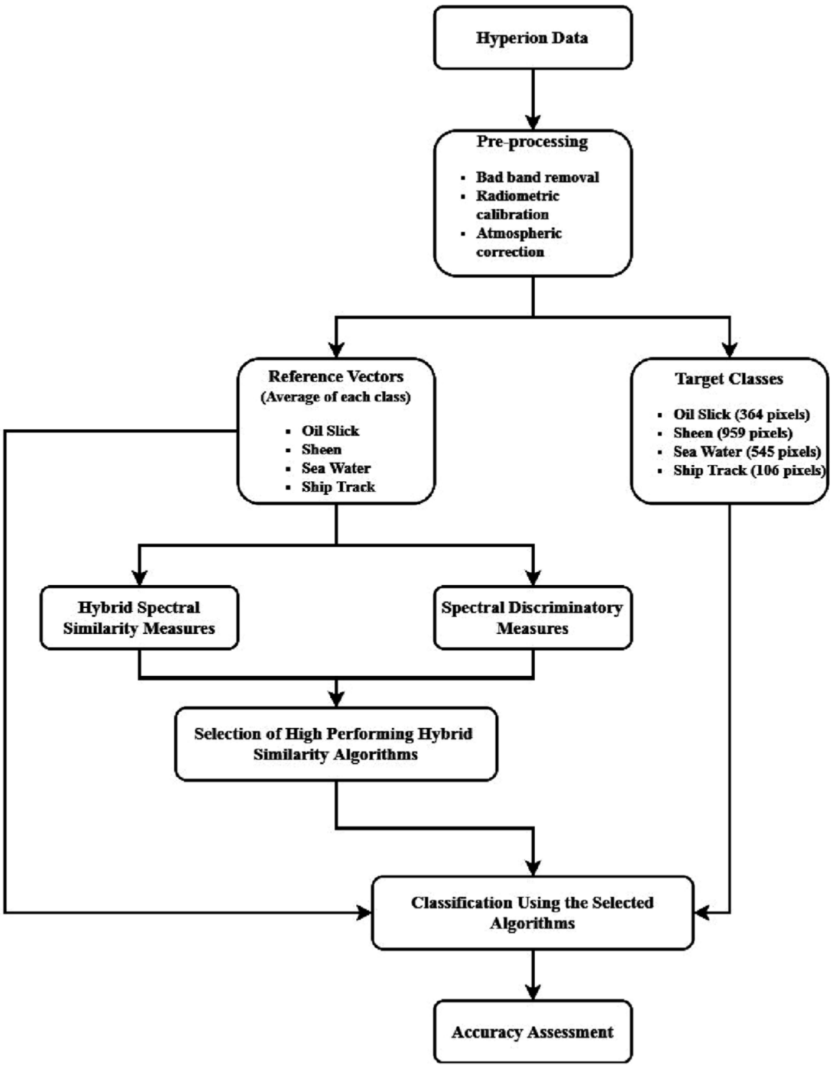

Figure 2. Technical flow chart.

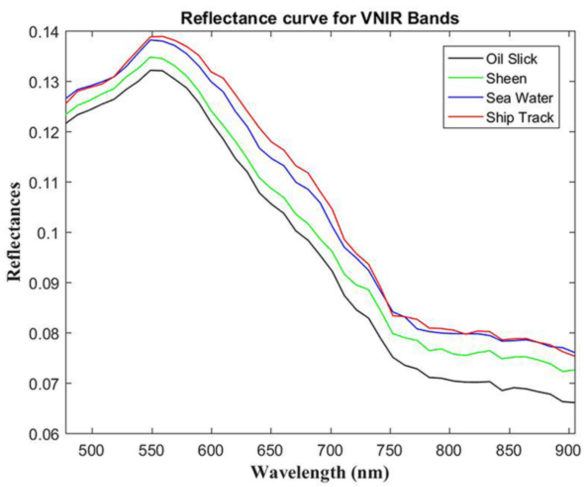

Figure 3. The reflectance curve for Oil Slick (O), Sheen (H), Sea Water (S) and Ship Track (T) spectra.

interpretation, SIM not only defines the randomness of a pixel but can also generate high-order statistics of the pixel from the spectral signatures Oil Slick (O), Sheen (H), Sea Water (S) and Ship Track (T) as in Table. 1. From the results, significant differences are not perceived between the moment values, realising the need for a better spectral discriminatory procedure.

Development of novel hybrid similarity measures

To facilitate the development of suitable hybrid similarity or discriminatory algorithms for efficient oil spill detection and to quantify it using hyperspectral imagery, this research appraises the advantages of the CHI method. For each hyperspectral image acquired at a particular wavelength λ_i, the pixel vector is represented as $r = (r_1, r_2, r_3, \ldots \ldots r_L)$ where each component r_i, represents a pixel in band

Table 1. Four moments produced by SIM for four spectral signatures in Figure 3.

Classes	Mean	Variance	Skewness	Kurtosis
Oil Slick	0.10269	0.000578	−3.97E-06	4.90E-07
Sheen	0.105793	0.000515	−2.55E-06	3.80E-07
Sea Water	0.109928	0.000514	−3.32E-06	3.83E-07
Ship Track	0.111169	0.000525	−4.24E-06	4.10E-07

image *Bi*. The corresponding spectral signature of r is defined as $s = (s_1,s_2,s_3, \dots \dots s_L)$ where s_i represents the spectral signature of r_i in the form of either radiance or reflectance values, and L is the total number of bands. Hence the chi-square distance (CHI or χ^2) between two spectral signatures $s_i = (s_{i1},s_{i2}, \dots \dots s_{il})$ and $s_j = (s_{j1},s_{j2}, \dots \dots s_{jl})$ is formulated as

$$\chi^2_{(s_i,s_j)} = \frac{1}{2}\sum_{l=1}^{L}\frac{\left(s_{il}-s_{jl}\right)^2}{\left(s_{il}+s_{jl}\right)} \tag{1}$$

Here, using Equation 1, four new CHI hybrid algorithms are developed by orthogonally projecting the spectral capabilities of individual measures and the tangent function. The newly developed hybrid similarity measures or algorithms provided in Equations 2–5 are compared and evaluated quantitatively with other existing hybrid similarity algorithms, namely CBD-SAM, CBD-SCM, EUD-SAM, EUD-SCM, JMD-CBD, JMD-EUD, JMD-SAM, JMD-SCM, SID-CBD, SID-EUD, SID-SAM and SID-SCM to assess their classification performance.

$$\text{CHI-SAM} = \text{CHI} \times \tan(\text{SAM}) \tag{2}$$

$$\text{CHI-SCM} = \text{CHI} \times \tan(\text{SCM}) \tag{3}$$

$$\text{JMD-CHI} = \text{JMD} \times \tan(\text{CHI}) \tag{4}$$

$$\text{SID-CHI} = \text{SID} \times \tan(\text{CHI}) \tag{5}$$

Spectral discriminability measures

The spectral similarity measures could measure the similarity or dissimilarity between any two pixel-vectors only, but this procedure alone is not sufficient to discriminate when there are more than two pixel-vectors or spectral-classes. This study defines an objective statistical criterion to evaluate the performance of all the hybrid similarity measures based on the spectral discriminatory statistics, namely RSDPW, RSDPB and RSDE. In order to compare the effectiveness between two hybrid similarity measures, the relative spectral discriminatory power (RSDPW) is formulated. It calculates the spectral discriminatory power of one pixel-vector from another relative to a reference pixel vector. Assume that $m(.,.)$ is a spectral measure, d is the reference spectral signature and s_i and s_j are the spectral signatures of any pair of two pixel-vectors that is used to classify d. Then, the relative spectral discriminatory power is given as

$$\text{RSDPW}_m\left(s_i,s_j;d\right) = \max\left\{\frac{m\left(s_i,d\right)}{m\left(s_j,d\right)},\frac{m\left(s_j,d\right)}{m\left(s_i,d\right)}\right\} \tag{6}$$

Obviously, the higher the $\text{RSDPW}_m(s_i,s_j;d)$, the better the discrimination power of the similarity measure $m(.,.)$.

To identify a pixel vector of interest or target spectrum, t, from an existing database or a spectral library Δ, another criterion called relative spectral discriminatory probability (RSDPB) is needed.

The RSDPB of all s_k in Δ relative to t is:

$$P_{t,}\Delta(k) = {m\left(t,s_k\right)} \Big/ {\sum_{j=1}^{L} m\left(t,s_j\right)} \tag{7}$$

For $k = 1, \dots, K$; where $m(.,.)$ is any of the similarity measure functions; t is the target spectrum; $\{s_k\}_{k=1}^{K}$ is the K spectral signatures in the database Δ. The resulting probability vector $P_{t,}\Delta = [P_{t,}\Delta(1),P_{t,}\Delta(2),P_{t,}\Delta(3), \dots \dots,P_{t,}\Delta(k)]^{\mathrm{T}}$, is called the relative spectral discriminatory probability vector of Δ relative to t. Then the target spectrum t is identified by selecting the one with the smallest relative spectral discriminatory probability, thereby t and the selected one will have the minimum spectral discrimination.

An uncertainty measure called relative spectral discriminatory entropy (RSDE) derived from RSDPB measures the uncertainty of identifying the target spectral signature t in the database Δ. The spectral discriminatory entropy of Δ with respect to t is given by

$$H_{\text{RSDE,}}\left(t;\Delta\right) = -\sum_{k=1}^{K} P_{t,\Delta}\left(k\right)\log P_{t,\Delta}\left(k\right) \tag{8}$$

where $P_{t,}(k)$ is the spectral discriminatory probability of t using the spectral database Δ. The smaller the $H_{RSDE,}(t;\Delta)$, the better is the chance to identify t.

Selection of high performing hybrid similarity algorithm

The ranks mentioned in Tables 3–7 based on RSDPW, RSPB and RSDE emphasise the significance of classifiers in discrimination of relative performances from hyperspectral images. For this perspective, the reference vector generated for each class is used to classify the target vector by applying the respective hybrid similarity algorithms.

Supervised classification and accuracy assessment

The selected hybrid similarity methods are extended in a supervised framework for improved pixel-based classification of the Hyperion image. Now, in this spectral matching based classification approach, each pixel in the sampling area is considered as a target spectrum, which is then compared with the reference vectors to generate classified images. The target is labelled to the corresponding reference spectrum according to the least matching value obtained, from which the confusion matrices are generated. Based on the confusion matrix, the overall accuracy (OA) of the classifiers is produced and is used for performance comparison. Additionally, the statistical results are manifested back to the hyperspectral subset to understand the real-world significance of classifier performances. Also, the importance of the VNIR range in hyperspectral oil spill analysis is highlighted with a comparative study between classifiers.

Results and discussion

In this paper, initially, the CHI-based hybrid similarity algorithms, CHI-SAM, CHI-SCM, JMD-CHI and SID-CHI, are compared with the existing hybrid similarity methods, CBD-SAM, CBD-SCM, EUD-SAM, EUD-SCM, JMD-CBD, JMD-EUD, JMD-SAM, JMD-SCM, SID-CBD, SID-EUD, SID-SAM and SID-SCM, to determine their capabilities to classify Oil Slick, Sheen, Sea Water and Ship Track spectral classes using spectral similarity and discriminatory statistics. Table 2 shows the results of hybrid spectral similarity values between Oil Slick, Sheen, Sea Water and Ship Track. Here, the high values specify better discrimination and the least value identifies a high similarity between the vectors.

Table 2 shows the spectral similarity values among four classes obtained by different hybrid spectral similarity measures. These similarity algorithms cannot help

Table 2. Similarity values produced based on different hybrid similarity measures between spectral signature pairs of Oil Slick (O), Sheen (H), Sea Water (S) and Ship Track (T).

Methods	O-H	O-S	O-T	H-S	H-T	S-T
CBD-SAM	0.175011	0.359529	0.407419	0.184515	0.232405	0.047888
CBD-SCM	0.175008	0.359533	0.407536	0.184548	0.232678	0.047983
CHI-SAM	9.49E-07	5.48E-06	8.34E-06	7.20E-07	2.08E-06	8.97E-08
CHI-SCM	5.47E-07	6.04E-06	1.56E-05	2.01E-06	6.51E-06	2.93E-07
EUD-SAM	0.028718	0.056251	0.064511	0.02953	0.039141	0.01145
EUD-SCM	0.028695	0.056273	0.065241	0.029733	0.040732	0.011842
JMD-CBD	0.002379	0.006676	0.008238	0.001359	0.002735	0.000288
JMD-CHI	5.20E-07	2.86E-06	4.17E-06	3.49E-07	9.96E-07	4.50E-08
JMD-EUD	0.000386	0.000999	0.001232	0.000215	0.000452	6.87E-05
JMD-SAM	0.000331	0.000605	0.000729	0.000109	0.000279	7.17E-05
JMD-SCM	0.00019	0.000667	0.001365	0.000305	0.000873	0.000234
SID-CBD	0.000128	0.000474	0.000629	3.96E-05	0.000126	6.91E-06
SID-CHI	2.80E-08	2.03E-07	3.18E-07	1.02E-08	4.61E-08	1.08E-09
SID-EUD	2.08E-05	7.10E-05	9.41E-05	6.27E-06	2.09E-05	1.65E-06
SID-SAM	1.78E-05	4.30E-05	5.57E-05	3.19E-06	1.29E-05	1.72E-06
SID-SCM	1.03E-05	4.74E-05	0.000104	8.88E-06	4.03E-05	5.62E-06

us to define conclusively any suitable hybrid measures[59] to discriminate oil spill classes, because spectral similarity measures calculate the similarity or dissimilarity between two spectral signatures only. In addition, these paired discrimination procedures cannot completely determine differences between more than two spectral classes effectively.[41] Moreover, as they use different measurement units, the performances can only be evaluated with comparable statistics. Now it becomes essential to use spectral discriminatory statistics like RSDPW, RSDPB and RSDE that can check the effectiveness of all the spectral similarity algorithms to classify a set of spectral classes based on a set of selected reference vectors. RSDPW, RSDPB and RSDE values also select the best hybrid spectral similarity algorithms for further hyperspectral image classification. Spectral discriminatory measures deliver authenticity and precision of comparison.[47]

Tables 3a and 3b show the result of RSDPW for the four spectral classes, viz. Oil Slick (O), Sheen (H), Sea Water (S) and Ship Track (T). In the table, the abbreviations in the column stand for various combinations of the four classes. For example, in the case of RSDPW of CBD-SAM, (H,S;O) denotes the spectral discrimination capability of CBD-SAM between the spectral signatures of Sheen (H) and Sea Water (S) relative to the reference spectral signature, Oil Slick (O). The higher value obtained for RSDPW is taken as a demonstration of the power of that particular measure. Similarly, all other combinations must be read. Here the performance rankings for the best five hybrid measures (bold) are identified inside the columns in brackets.

Tables 3a and 3b show the RSDPW values of all the hybrid classifiers. From these values, the best hybrid similarity measures are selected based on analysing their ranks and their overall occurrence in different combinations. In the case of Oil Slick or Sheen as the reference vector, the hybrid measures CHI-SCM, CHI-SAM, SID-SCM, SID-CHI and JMD-CHI are selected based on their higher-ranking values. For Sea Water or Ship Track as the reference vector, the selected hybrid measures are SID-CHI, SID-CBD, JMD-CHI, CHI-SAM, SID-EUD, which achieved promising values.

To compute the RSDPB and RSDE for evaluating which measure is more effective, mixed spectral signatures or mixtures are generated to use as the target signature (*t*) for identification. Note that target signature (*t*) is generated randomly.[41,58,60] Here, the database is made up of a mixture of four classes Δ = {Oil Slick, Sheen, Sea Water, Ship Track}. Four trials are conducted, in the first trial (mixture 1), the target signature is composed of 0.8125 Oil Slick and the remaining 0.1875 comprising all the

Table 3a. Relative Spectral Discriminatory Power (RSDPW) values produced for Oil Slick (O) and Sheen (H) as reference vectors. Best five hybrid measures are bolded.

Methods	(H,S;O)	(H,T;O)	(S,T;O)	(S,O;H)	(O,T;H)	(S,T;H)
CBD-SAM	2.0543	2.3280	1.1332	1.0543	1.3279	1.2595
CBD-SCM	2.0544	2.3287	1.1335	1.0545	1.3295	1.2608
CHI-SAM	**5.7774 (3)**	**8.7909 (4)**	**1.5216 (5)**	**1.3191**	**2.1932 (4)**	2.8930
CHI-SCM	**11.0499 (1)**	**28.5600 (1)**	**2.5846(1)**	**3.6676 (2)**	**11.9098 (1)**	**3.2473 (5)**
EUD-SAM	1.9587	2.2463	1.1468	1.0283	1.3630	1.3255
EUD-SCM	1.9611	2.2736	1.1594	1.0362	1.4194	1.3699
JMD-CBD	2.8060	3.4623	1.2339	1.7503	1.1494	2.0118
JMD-CHI	**5.5016 (4)**	**8.0210 (5)**	1.4579	1.4900	**1.9166 (5)**	2.8556
JMD-EUD	2.5877	3.1897	1.2326	1.7953	1.1711	2.1026
JMD-SAM	1.8298	2.2054	1.2053	**3.0219 (5)**	1.1851	2.5498
JMD-SCM	3.4997	7.1651	**2.0473 (3)**	1.6009	**4.5819 (2)**	2.8620
SID-CBD	3.7040	4.9115	1.3260	3.2339 (4)	1.0132	3.1917
SID-CHI	**7.2624 (2)**	**11.3785 (2)**	**1.5668 (4)**	2.7529	1.6457	**4.5305 (2)**
SID-EUD	3.4159	4.5248	1.3246	**3.3170 (3)**	1.0056	**3.3357 (4)**
SID-SAM	2.4154	3.1286	1.2952	**5.5832 (1)**	1.3802	**4.0452 (3)**
SID-SCM	**4.6198 (5)**	**10.1643 (3)**	**2.2002 (2)**	1.1541	**3.9344 (3)**	**4.5406 (1)**

Table 3b. Relative Spectral Discriminatory Power (RSDPW) values produced for Sea Water (S) and Ship Track (T) as reference vectors. Best five hybrid measures are bolded.

Methods	(H,O;S)	(T,H;S)	(T,O;S)	(H,O;T)	(S,O;T)	(S,H;T)
CBD-SAM	1.9485	7.5077	3.8531	1.7531	8.5078	4.8531
CBD-SCM	1.9482	7.4929	3.8461	1.7515	8.4933	4.8492
CHI-SAM	7.6207	**61.1323 (4)**	**8.0219 (2)**	4.0082	**93.0188 (2)**	**23.2073 (2)**
CHI-SCM	3.0128	20.6504	**6.8542 (4)**	2.3980	53.3739	**22.2573 (3)**
EUD-SAM	1.9049	4.9126	2.5790	1.6481	5.6340	3.4184
EUD-SCM	1.8926	4.7519	2.5108	1.6017	5.5091	3.4395
JMD-CBD	4.9114	23.2113	4.7260	3.0122	28.6402	9.5079
JMD-CHI	**8.1973 (5)**	**63.4979 (3)**	**7.7462 (3)**	**4.1851 (5)**	**92.5762 (3)**	**22.1203 (4)**
JMD-EUD	4.6458	14.5461	3.1310	2.7236	17.9300	6.5833
JMD-SAM	5.5295	8.4327	1.5250	2.6137	10.1638	3.8886
JMD-SCM	2.1861	2.8486	1.3031	1.5638	5.8319	3.7294
SID-CBD	**11.9784 (3)**	**68.6979 (2)**	**5.7351 (5)**	**4.9764 (2)**	**91.0930 (4)**	**18.3051 (5)**
SID-CHI	**19.9925 (1)**	**187.9329 (1)**	**9.4002 (1)**	**6.9140 (1)**	**294.4480 (1)**	**42.5870 (1)**
SID-EUD	**11.3306 (4)**	**43.0516 (5)**	3.7996	**4.4995 (3)**	**57.0282 (5)**	12.6745
SID-SAM	**13.4858 (2)**	24.9581	1.8507	**4.3180 (4)**	32.3269	7.4865
SID-SCM	5.3316	8.4308	1.5813	2.5834	18.5490	7.1800

other three spectra in equal proportion. For the second trial (mixture 2), the target signature is composed of 0.8125 Sheen, and the remaining 0.1875 is the other three spectra in equal proportion. In the third trial (mixture 3), the target signature is composed of 0.8125 Sea Water and the remaining 0.1875 for the remaining three spectra in equal proportion. Likewise, in the fourth trial (mixture 4), the target signature is composed of 0.8125 Ship Track and the remaining 0.1875 for the other three spectra in equal proportion. Tables 4–7 show the relative spectral discriminatory probability vectors and RSDE of the spectral signatures in the database when compared with the mixture *t*. From the RSDPB table, the target signature (*t*) can be identified from the database Δ which has the smallest probability value. For RSDE, ranks are assigned to the classifiers to identify the best performing algorithms based on entropy values. The lower the entropy value, the higher is the chance of getting correctly matched targets.

From Table 4, for RSDPB, it is evident that the Oil Slick spectra and the mixture *t* represented as (O-*t*), i.e. the first column of Table 4, has the minimum spectral discrimination probability, highlighting the prominence of Oil Slick in mixture 1. Here, the mixture 1 entropy shows the least uncertainty value 0.9554 for the CHI-SCM hybrid similarity measure followed by the hybrids SID-CHI, CHI-SAM, SID-SCM and JMD-CHI attaining values of 1.1183, 1.1834, 1.1893 and 1.2044, respectively.

From Table 5, for RSDPB, it is clear that the Sheen spectra and the mixture *t* represented as (H-*t*), i.e. the second column of Table 5, have the minimum spectral discrimination probability, highlighting the prominence of Sheen in mixture 2. In mixture 2, the least entropy is obtained for CHI-SCM with a value of 1.0920, followed by SID-SCM, SID-SAM, JMD-SCM and SID-CHI retaining values of 1.2285, 1.2879, 1.3365 and 1.3593, respectively.

From Table 6, for RSDPB, it is apparent that the Sea Water spectra and the mixture *t* represented as (S-*t*), i.e. the third column of Table 6. have the minimum spectral discrimination probability, highlighting the prominence of Sea Water in mixture 3. In mixture 3, SID-CHI produced the least entropy value of 0.3209, followed by SID-CBD, SID-EUD, SID-SAM and JMD-CHI with values of 0.5259, 0.5723, 0.5902 and 0.6285, respectively.

From Table 7, for RSDPB, it is seen that the Ship Track spectra and the mixture *t* represented as (T-*t*), i.e. the fourth column of Table 7, have the minimum spectral discrimination probability, highlighting the prominence of Ship Track in mixture 4. Here, again SID-CHI produced the least entropy value 0.4726, followed by SID-CBD,

Table 4. Relative spectral discriminatory probability vectors produced by the hybrid similarity measures with the target *t* chosen to be a mixture of 0.8125 Oil Slick, 0.0625 Sheen, 0.0625 Sea Water and 0.0625 Ship Track (Mixture 1).

Methods	O-*t*	H-*t*	S-*t*	T-*t*	RSDE
CBD-SAM	0.0714	0.1409	0.3648	0.4229	1.7261
CBD-SCM	0.0714	0.1409	0.3647	0.4230	1.7261
CHI-SAM	0.0032	0.0391	0.3599	0.5979	**1.1834 (3)**
CHI-SCM	0.0020	0.0197	0.2457	0.7327	**0.9554 (1)**
EUD-SAM	0.0703	0.1515	0.3575	0.4207	1.7378
EUD-SCM	0.0700	0.1507	0.3559	0.4234	1.7354
JMD-CBD	0.0162	0.1045	0.3841	0.4952	1.4692
JMD-CHI	0.0033	0.0426	0.3698	0.5844	**1.2044 (5)**
JMD-EUD	0.0165	0.1157	0.3781	0.4896	1.4928
JMD-SAM	0.0175	0.1753	0.3553	0.4519	1.5906
JMD-SCM	0.0122	0.0983	0.2709	0.6186	1.3455
SID-CBD	0.0036	0.0749	0.3811	0.5404	1.3193
SID-CHI	0.0007	0.0295	0.3542	0.6157	**1.1183 (2)**
SID-EUD	0.0037	0.0833	0.3766	0.5364	1.3409
SID-SAM	0.0039	0.1289	0.3614	0.5057	1.4406
SID-SCM	0.0026	0.0693	0.2642	0.6638	**1.1893 (4)**

Table 5. Relative spectral discriminatory probability vectors produced by the hybrid similarity measures with the target *t* chosen to be a mixture of 0.8125 Sheen, 0.0625 Oil Slick, 0.0625 Sea Water and 0.0625 Ship Track (Mixture 2).

Methods	O-*t*	H-*t*	S-*t*	T-*t*	RSDE
CBD-SAM	0.3212	0.0255	0.2862	0.3671	1.7087
CBD-SCM	0.3211	0.0255	0.2861	0.3673	1.7086
CHI-SAM	0.3340	0.0004	0.1619	0.5037	1.4566
CHI-SCM	0.0795	0.0006	0.1945	0.7255	**1.0920 (1)**
EUD-SAM	0.3161	0.0306	0.2777	0.3756	1.7229
EUD-SCM	0.3120	0.0302	0.2753	0.3825	1.7194
JMD-CBD	0.4200	0.0032	0.1874	0.3895	1.5345
JMD-CHI	0.3616	0.0004	0.1580	0.4801	1.4640
JMD-EUD	0.4146	0.0039	0.1830	0.3985	1.5349
JMD-SAM	0.4922	0.0049	0.1376	0.3653	1.4652
JMD-SCM	0.1436	0.0087	0.2027	0.6450	**1.3365 (4)**
SID-CBD	0.5065	0.0004	0.1134	0.3797	1.3879
SID-CHI	0.4361	0.0000	0.0957	0.4681	**1.3593 (5)**
SID-EUD	0.5002	0.0004	0.1108	0.3886	1.3865
SID-SAM	0.5743	0.0005	0.0806	0.3445	**1.2879 (3)**
SID-SCM	0.1871	0.0011	0.1325	0.6793	**1.2285 (2)**

JMD-CHI, SID-EUD and CHI-SAM having values of 0.5993, 0.6788, 0.6832 and 0.6931 respectively. Thus, it is evident from the above Tables 4–7 that SID-CHI, CHI-SCM, SID-CBD, SID-SCM, JMD-CHI, CHI-SAM, SID-EUD and SID-SAM are the best among all the hybrid measures tested for uncertainty.

Overall, the higher ranks of CHI-based hybrid similarity measures, viz. SID-CHI, JMD-CHI, CHI-SAM and

Table 6. Relative spectral discriminatory probability vectors produced by the hybrid similarity measures with the target *t* chosen to be a mixture of 0.8125 Sea Water, 0.0625 Oil Slick, 0.0625 Sheen and 0.0625 Ship Track (Mixture 3).

Methods	O-*t*	H-*t*	S-*t*	T-*t*	RSDE
CBD-SAM	0.5550	0.2593	0.0524	0.1333	1.5868
CBD-SCM	0.5549	0.2593	0.0524	0.1334	1.5870
CHI-SAM	0.8736	0.0934	0.0006	0.0324	0.6566
CHI-SCM	0.7144	0.2060	0.0006	0.0790	1.1121
EUD-SAM	0.5349	0.2588	0.0503	0.1560	1.6225
EUD-SCM	0.5321	0.2592	0.0500	0.1588	1.6268
JMD-CBD	0.7883	0.1383	0.0059	0.0674	0.9714
JMD-CHI	0.8814	0.0873	0.0006	0.0307	**0.6285 (5)**
JMD-EUD	0.7679	0.1436	0.0059	0.0826	1.0358
JMD-SAM	0.7616	0.1229	0.0051	0.1104	1.0610
JMD-SCM	0.5331	0.2320	0.0045	0.2304	1.4958
SID-CBD	0.9091	0.0617	0.0006	0.0287	**0.5259 (2)**
SID-CHI	0.9513	0.0364	0.0001	0.0122	**0.3209 (1)**
SID-EUD	0.8988	0.0650	0.0006	0.0356	**0.5723 (3)**
SID-SAM	0.8958	0.0559	0.0005	0.0479	**0.5902 (4)**
SID-SCM	0.7528	0.1266	0.0005	0.1200	1.0586

Table 7. Relative spectral discriminatory probability vectors produced by the hybrid similarity measures with target *t* chosen to be a mixture of 0.8125 Ship Track, 0.0625 Oil Slick, 0.0625 Sheen and 0.0625 Sea Water (Mixture 4).

Methods	O-*t*	H-*t*	S-*t*	T-*t*	RSDE
CBD-SAM	0.6056	0.3148	0.0082	0.0714	1.2916
CBD-SCM	0.6052	0.3148	0.0086	0.0714	1.2940
CHI-SAM	0.8295	0.1660	0.0030	0.0015	**0.6931 (5)**
CHI-SCM	0.7290	0.2642	0.0047	0.0021	0.8948
EUD-SAM	0.5567	0.3112	0.0643	0.0678	1.5122
EUD-SCM	0.5520	0.3161	0.0650	0.0668	1.5157
JMD-CBD	0.7699	0.2178	0.0028	0.0096	0.8570
JMD-CHI	0.8357	0.1597	0.0032	0.0014	**0.6788 (3)**
JMD-EUD	0.7352	0.2313	0.0236	0.0099	1.0081
JMD-SAM	0.7047	0.2339	0.0524	0.0090	1.1303
JMD-SCM	0.5707	0.3429	0.0744	0.0120	1.3468
SID-CBD	0.8609	0.1371	0.0009	0.0012	**0.5993 (2)**
SID-CHI	0.9019	0.0970	0.0010	0.0002	**0.4726 (1)**
SID-EUD	0.8421	0.1491	0.0075	0.0012	**0.6832 (4)**
SID-SAM	0.8272	0.1546	0.0171	0.0012	0.7545
SID-SCM	0.7263	0.2457	0.0263	0.0017	0.9862

CHI-SCM, emphasise their strong performance in spectral discrimination analysis of hyperspectral images. The selected hybrid similarity methods, namely SID-CHI, CHI-SCM, SID-CBD, SID-SCM, JMD-CHI, CHI-SAM, SID-EUD and SID-SAM, are extended in a supervised framework for improved pixel-based classification of the Hyperion image. The target pixels or unknown image pixels are collected from the locations shown in Figure 4.

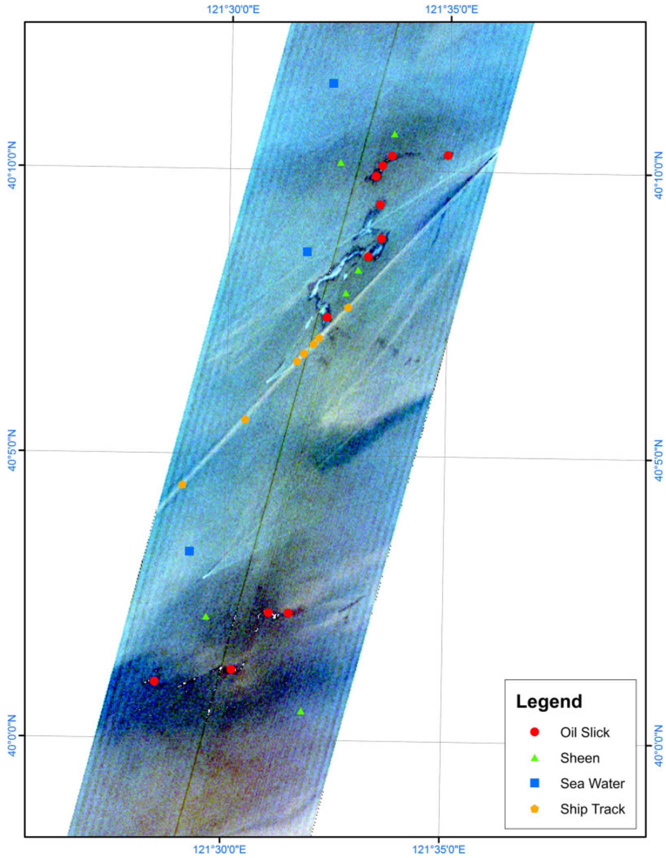

Figure 4. Sampling locations of hyperspectral targets of marine spectral classes, viz. Oil Slick (O), Sheen (H), Sea Water (S) and Ship Track (T).

The confusion matrix results from Table 8 have produced considerably higher overall accuracy for JMD-CHI (85 %) followed by the other CHI-based hybrids, namely CHI-SAM (84 %), CHI-SCM (83 %) and SID-CHI (82 %). Together with the discriminatory statistics output, the results demonstrated the superiority of the developed CHI hybrid spectral similarity measures.

The resultant images in Figure 5 show how the different CHI hybrids performed while classifying Hyperion imagery (supplementary Figure S1 shows the classification result for the subset shown in Figure 4). Notably, all the classes are correctly identified and delineated. The violet colour produced outside the Ship Track is due to the SPM prominent in the Sea Water. For further ratification, the overall accuracy of the CHI-based hybrids is tested for the SWIR, and all bands in Hyperion's range.

The values of overall accuracy for the CHI algorithms in Table 9 confirm that the VNIR bands produced higher OA, recommending the usage of VNIR bands in detecting crude oil spills.

Previous research based on spectral similarities exposed more details on individual spectral similarity measures, but only a very few ventured into hyperspectral remote sensing applications like marine oil spill detection. Our research developed novel CHI hybrid spectral similarity methods that combined the strengths of individual algorithms, which were compared and tested for their discrimination capability. The promising results explicitly obtained by CHI-based hybrids and their superiority in the VNIR spectral range indicate the need for more studies in the hyperspectral characterisation of marine oil spill detection.

Conclusion

Hyperspectral imagery brings the capability to collect minute details of the sea surface that, when combined with suitable processing and analysis techniques, serves as a tool for the continuous monitoring of an oil spill. In

Table 8. The confusion matrix for the selected hybrid similarity measures.

Method		Reference data					
		Classes	Oil Slick	Sheen	Sea Water	Ship Track	Overall accuracy
CHI-SAM	Classified data	Oil Slick	310	1	0	0	84 %
		Sheen	54	958	59	2	
		Sea Water	0	0	321	25	
		Ship Track	0	0	165	79	
CHI-SCM		Oil Slick	305	1	0	0	83 %
		Sheen	59	958	94	7	
		Sea Water	0	0	286	0	
		Ship Track	0	0	165	99	
JMD-CHI		Oil Slick	310	1	0	0	85 %
		Sheen	54	958	55	1	
		Sea Water	0	0	325	26	
		Ship Track	0	0	165	79	
SID-CBD		Oil Slick	321	1	0	0	80 %
		Sheen	43	958	143	3	
		Sea Water	0	0	237	30	
		Ship Track	0	0	165	73	
SID-CHI		Oil Slick	317	1	0	0	82 %
		Sheen	47	958	113	2	
		Sea Water	0	0	267	24	
		Ship Track	0	0	165	80	
SID-EUD		Oil Slick	324	2	0	0	78 %
		Sheen	40	957	197	3	
		Sea Water	0	0	183	23	
		Ship Track	0	0	165	80	
SID-SAM		Oil Slick	331	3	0	0	74 %
		Sheen	33	956	287	5	
		Sea Water	0	0	93	17	
		Ship Track	0	0	165	84	
SID-SCM		Oil Slick	331	3	0	0	74 %
		Sheen	31	956	287	4	
		Sea Water	2	0	93	20	
		Ship Track	0	0	165	82	

this study, the investigation of the very high-resolution hyperspectral image from Hyperion is performed to analyse marine oil spill-related spectra through photo-interpretation. This is carried out with regard to the hybrid spectral similarity approach emphasising the capability of CHI-based hybrid algorithms. The oil spill detection method based on spectral similarity generated a reference vector for each class, Oil Slick, Sheen, Sea Water and Ship Track, using the average values of pixels for each of the 43 channels. The similarity matching measure and the respective spectral discriminatory statistics RSDPW, RSDPB and RSDE enabled the selection of eight efficient hybrid similarity measures. After the classification and accuracy assessment, it can be seen that the CHI-based hybrid classifier JMD-CHI produced the highest OA of 85 %, followed by CHI-SAM, CHI-SCM and SID-CHI

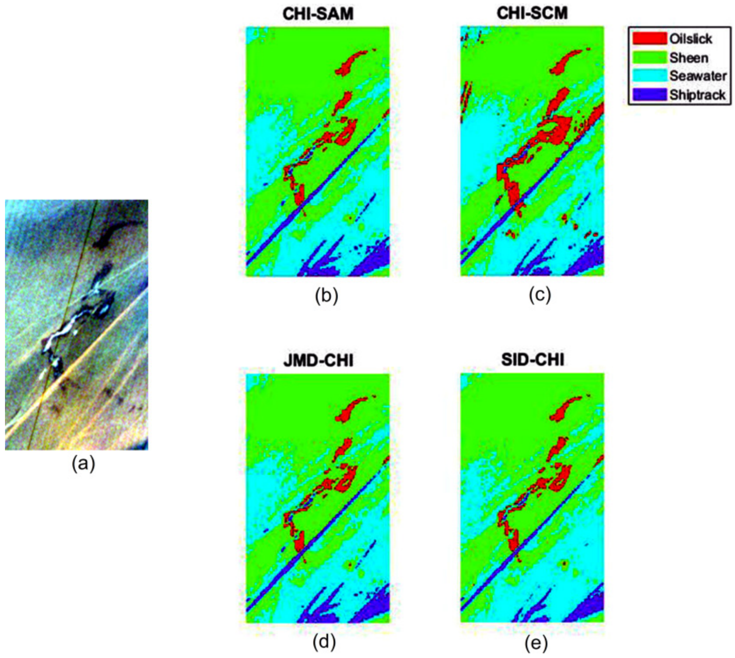

Figure 5. The training subset (a) and the resultant classified images (b–e) for the CHI-based hybrid similarity measures.

Table 9. Comparative results for the overall accuracy of CHI-based hybrid similarity measures.

Methods	VNIR	SWIR	All Bands
CHI-SAM	84 %	66 %	76 %
CHI-SCM	83 %	68 %	78 %
JMD-CHI	85 %	67 %	78 %
SID-CHI	82 %	67 %	77 %

with OA of 84 %, 83 % and 82 %, respectively. Overall, the supervised classification methodology allowed the delineation of the target spectrum into respective classes serving as the best evidence for the performance evaluation of the developed CHI hybrids. Our results have shown that the systematic application of the developed chi-square distance-based similarity measures on hyperspectral images revealed detailed information on oil spills in the sea.

Author contributions

Conceptualisation, methodology, formal analysis, writing (original draft preparation), writing (review and editing), Deepthi. Supervision, Project administration, Tessamma Thomas. All authors have read and agreed to the published version of the manuscript.

Funding

This research did not receive any funding.

Conflicts of interest

The authors declare no conflict of interest.

References

1. K. Grüner, R. Reuter and H. Smid, "A new sensor system for airborne measurements of maritime pollution and of hydrographic parameters", *GeoJournal* **24(1),** 103–117 (1991). https://doi.org/10.1007/BF00213062
2. Y.-H. Jung, H.-S. Park, K.-T. Yoon, H.-J. Kim and W.-J. Shim, "Long-term changes in rocky intertidal macrobenthos during the five years after the Hebei Spirit oil spill, Taean, Korea", *Ocean Sci. J.* **52(1),**

103–112 (2017). https://doi.org/10.1007/s12601-017-0008-5

3. J. Shi, J. Jiao, Y. Lu, M. Zhang, Z. Mao and Y. Liu, "Determining spectral groups to distinguish oil emulsions from Sargassum over the Gulf of Mexico using an airborne imaging spectrometer", *ISPRS J. Photogram. Remote Sens.* **146,** 251–259 (2018). https://doi.org/10.1016/j.isprsjprs.2018.09.017
4. K. Ryan and K. Ali, "Application of a partial least-squares regression model to retrieve chlorophyll-*a* concentrations in coastal waters using hyper-spectral data", *Ocean Sci. J.* **51(2),** 209–221 (2016). https://doi.org/10.1007/s12601-016-0018-8
5. J.M. Bioucas-Dias, A. Plaza, G. Camps-Valls, P. Scheunders, N. Nasrabadi and J. Chanussot, "Hyperspectral remote sensing data analysis and future challenges", *IEEE Geosci. Remote Sens. Mag.* **1(2),** 6–36 (2013). https://doi.org/10.1109/MGRS.2013.2244672
6. D. Zhao, X. Cheng, H. Zhang, Y. Niu, Y. Qi and H. Zhang, "Evaluation of the ability of spectral indices of hydrocarbons and seawater for identifying oil slicks utilizing hyperspectral images", *Remote Sens.* **10(3),** 421 (2018). https://doi.org/10.3390/rs10030421
7. L. Cong, B. Nutter and D. Liang, "Estimation of oil thickness and aging from hyperspectral signature", *2012 IEEE Southwest Symposium on Image Analysis and Interpretation*, Santa Fe, NM, pp. 213–216 (2012). https://doi.org/10.1109/SSIAI.2012.6202491
8. D. Palmer, G.A. Borstad and S. Boxall, "Airborne multispectral remote sensing of the January 1993 Shetlands oil spill", in *Proceedings of the Second Thematic Conference on Remote Sensing for Marine and Coastal Environments: Needs, Solutions and Applications*. ERIM, Ann Arbor, Vol. II, p. 546 (2011). https://remote-sensing.aslenv.com/documents/Airborne%20Multispectral%20Remote%20Sensing%20of.pdf
9. K. Polychronis and V. Karathanassi, "Detection of oil spills and underwater natural oil outflow using multi-spectral satellite imagery", *Int. J. Remote Sens. Appl.* **3,** 145–154 (2013).
10. I. Leifer, W.J. Lehr, D. Simecek-Beatty, E. Bradley, R. Clark, P. Dennison, Y. Hu, S. Matheson, C.E. Jones, B. Holt, M. Reif, D.A.Roberts, J. Svejkovsky, G. Swayze and J. Wozencraft, "State of the art satellite and airborne marine oil spill remote sensing: Application to the BP *Deepwater Horizon* oil spill", *Remote Sens. Environ.* **124,** 185–209 (2012). https://doi.org/10.1016/j.rse.2012.03.024
11. B. Liu, Y. Li and X. Zhu, "Assessing the capabilities of hyperspectral remote sensing to map oil films on waters", *Proc. SPIE* **9299,** 929902 (2014). https://doi.org/10.1117/12.2066293
12. B. Liu, Y. Li, Q. Zhang and L. Han, "Assessing sensitivity of hyperspectral sensor to detect oils with sea ice", *J. Spectrosc.* **2016,** 6584314 (2016). https://doi.org/10.1155/2016/6584314
13. M. Fingas and C. Brown, "Review of oil spill remote sensing", *Mar. Pollut. Bull.* **83(1),** 9–23 (2014). https://doi.org/10.1016/j.marpolbul.2014.03.059
14. R.D.P.M. Scafutto, C.R. de Souza Filho and W.J. de Oliveira, "Hyperspectral remote sensing detection of petroleum hydrocarbons in mixtures with mineral substrates: Implications for onshore exploration and monitoring", *ISPRS J. Photogram. Remote Sens.* **128,** 146–157 (2017). https://doi.org/10.1016/j.isprsjprs.2017.03.009
15. S.A. El-Rahman and A.H.S. Zolait, "Hyperspectral image analysis for oil spill detection: A comparative study", *Int. J. Comput. Sci. Math.* **9(2),** 103–121 (2018). https://doi.org/10.1504/IJCSM.2018.091744
16. Y.C. Lu, Q.J. Tian, X.P. Qi, J.J. Wang and X.C. Wang, "Spectral response analysis of offshore thin oil slicks", *Guang pu xue yu guang pu fen xi= Guang pu* **29(4),** 986–989 (2009) [in Chinese]. https://europepmc.org/article/med/19626887
17. A. Keshavarz and S.M. Karim Hashemizadeh, "Analysis of hyperspectral imagery for oil spill detection using SAM unmixing algorithm techniques", *Iranian J. Oil Gas Sci. Technol.* **6(2),** 1–16 (2017).
18. C. Pietrapertosa, A. Spisni, V. Pancioli, Pavan, P. Ssterzai, P. Paganini, M. Vellico, A. Monni and F. Coren, "Hyperspectral images to monitor oil spills in the River Po", *Bollettino di Geofisica Teorica ed Applicata* **57(1),** 31–42 (2016). https://doi.org/10.4430/bgta0172
19. D. Sykas, V. Karathanassi, C. Andreou and P. Kolokoussis, "Oil spill mapping using hyperspectral methods and techniques", *Proceedings of the 10th International Conference on the Mediterranean Coastal Environment, MEDCOAST 2011*, pp. 651–662 (2011). https://doi.org/10.13140/2.1.2674.1764

20. C. Cui, Y. Li, B. Liu and G. Li, "A new endmember preprocessing method for the hyperspectral unmixing of imagery containing marine oil spills", *ISPRS Int. J. Geo-Inform.* **6(9),** 286 (2017). https://doi.org/10.3390/ijgi6090286

21. D. Liu, J. Zhang and X. Wang, "Reference spectral signature selection using density-based cluster for automatic oil spill detection in hyperspectral images", *Optics Express* **24(7),** 7411 (2016). https://doi.org/10.1364/oe.24.007411

22. S. Asadzadeh, C.R. de Souza and C. Postal, "Review and categorization of spectral processing methods", *Anais XVII Simpósio Brasileiro de Sensoriamento Remoto - SBSR, João Pessoa-PB, Brasil, 25 a 29 de abril de 2015, INPE* **1,** 6381–6388 (2015).

23. B.R. Shivakumar and S.V. Rajashekararadhya, "Performance evaluation of spectral angle mapper and spectral correlation mapper classifiers over multiple remote sensor data", *2017 Second International Conference on Electrical, Computer and Communication Technologies (ICECCT)*, Coimbatore, pp. 1–6 (2017). https://doi.org/10.1109/ICECCT.2017.8117946

24. A.J. Brown, "Spectral curve fitting for automatic hyperspectral data analysis", *IEEE Trans. Geosci. Remote Sens.* **44(6),** 1601–1608 (2006). https://doi.org/10.1109/TGRS.2006.870435

25. A.J. Brown, S.J. Hook, A.M. Baldridge, J.K. Crowley, N.T. Bridges, B.J. Thomson, G.M. Marion, C.R. de Souza Filho and J.L. Bishop, "Hydrothermal formation of Clay-Carbonate alteration assemblages in the Nili Fossae region of Mars", *Earth Planetary Sci. Lett.* **297(1–2),** 174–182 (2010). https://doi.org/10.1016/j.epsl.2010.06.018

26. J.W. Boardman, F.A. Kruse and R.O. Green, "Mapping target signatures via partial unmixing of AVIRIS data", *Jet Propulsion* **23,** 23–26 (1993).

27. W. Pervez, S.A. Khan and Valiuddin, "Hyperspectral Hyperion imagery analysis and its application using spectral analysis", *Int. Arch. Photogramm. Remote Sens. Spatial Inf. Sci.* **XL-3/W2,** 169–175 (2015). https://doi.org/10.5194/isprsarchives-XL-3-W2-169-2015

28. A. Song, J. Choi, Y. Kim and Y. Kim, *Analysis of Appropriate Spectral Similarity Methods to Classify Target Species Using CASI Hyperspectral Images.* http://citeseerx.ist.psu.edu/viewdoc/download?doi=10.1.1.741.7892&rep=rep1&type=pdf

29. P. Du and Y. Chen, "A novel spectral similarity measure approach based on set operations and spectral polygon", *Proc. 2005 IEEE International Geoscience and Remote Sensing Symposium*, Seoul, pp. 4319–4322 (2005). https://doi.org/10.1109/IGARSS.2005.1525874

30. S. Padma and S. Sanjeevi, "Jeffries Matusita-Spectral Angle Mapper (JM-SAM) spectral matching for species level mapping at Bhitarkanika, Muthupet and Pichavaram mangroves", *Int. Arch. Photogramm. Remote Sens. Spatial Inf. Sci.* **XL-8,** 1403–1411 (2014). https://doi.org/10.5194/isprsarchives-XL-8-1403-2014

31. M.J. Swain and D.H. Ballard, "Color indexing", *Int. J. Comput. Vision.* **7(1),** 11–32 (1991). https://doi.org/10.1007/BF00130487

32. F.A. Kruse, A.B. Lefkoff, J.W. Boardman, K.B. Heidebrecht, A.T. Shapiro, P.J. Barloon and A.F.H. Goetz, "The spectral image processing system (SIPS)—interactive visualization and analysis of imaging spectrometer data", *Remote Sens. Environ.* **44(2),** 145–163 (1993). https://doi.org/10.1016/0034-4257(93)90013-N

33. J.C. Granahan and J.N. Sweet, "An evaluation of atmospheric correction techniques using the spectral similarity scale", *IGARSS 2001. Scanning the Present and Resolving the Future. Proceedings. IEEE 2001 International Geoscience and Remote Sensing Symposium (Cat. No.01CH37217)*, Sydney, NSW, Australia, Vol. 5, pp. 2022–2024 (2001). https://doi.org/10.1109/IGARSS.2001.977890

34. O.A. De Carvalho and P.R. Meneses, "Spectral correlation mapper (SCM): an improvement on the spectral angle mapper (SAM)", *Summaries of the 9th JPL Airborne Earth Science Workshop.* JPL Publication 00-18, Vol. 9 (2000).

35. C.-I. Chang, "An information-theoretic approach to spectral variability, similarity, and discrimination for hyperspectral image analysis", *IEEE Trans. Inform. Theory* **46(5),** 1927–1932 (2000). https://doi.org/10.1109/18.857802

36. L. Bruzzone, F. Roli and S.B. Serpico, "An extension of the Jeffreys-Matusita distance to multiclass cases for feature selection", *IEEE Trans. Geosci. Remote Sens.* **33(6),** 1318–1321 (1995). https://doi.org/10.1109/36.477187

37. S. Homayouni and M. Roux, "Hyperspectral image analysis for material mapping using spectral matching", *ISPRS Archives* Vol. XXXV, Part B7, pp. 49–54 (2004). https://www.isprs.org/proceedings/XXXV/congress/comm7/papers/10.pdf

38. Q. Li and C. Niu, "Feature-enhanced spectral similarity measure for the analysis of hyperspectral imagery", *J. Appl. Remote Sens.* **9(1),** 096008 (2015). https://doi.org/10.1117/1.jrs.9.096008

39. J. Granahan, "A compositional study of asteroid 243 Ida and Dactyl from Galileo NIMS and SSI observations", *J. Geophys. Res.* **107(E10),** 20-1–20-10 (2002). https://doi.org/10.1029/2001je001759

40. Y. Du, C.-I. Chang, H. Ren, C.-C. Chang, J.O. Jensen and F.M. D'Amico, "New hyperspectral discrimination measure for spectral characterization", *Optical Eng.* **43(8),** 1777–1786 (2004). https://doi.org/10.1117/1.1766301

41. M. Naresh Kumar, M.V.R. Seshasai, K.S. Vara Prasad, V. Kamala, K.V. Ramana, R.S. Dwivedi and P.S. Roy, "A new hybrid spectral similarity measure for discrimination among *Vigna* species", *Int. J. Remote Sens.* **32(14),** 4041–4053 (2011). https://doi.org/10.1080/01431161.2010.484431

42. S. Padma and S. Sanjeevi, "Jeffries Matusita based mixed-measure for improved spectral matching in hyperspectral image analysis", *Int. J. Applied Earth Obs. Geoinform.* **32,** 138–151 (2014). https://doi.org/10.1016/j.jag.2014.04.001

43. S. Padma and S. Sanjeevi, "Spectral correlation and Jeffries-Matusita based matching algorithm for improved information extraction from hyperspectral images", *Proceedings of 37th Asian Conference on Remote Sensing* (2016).

44. Deepthi and T. Thomas, "Performance comparison of hyperspectral oil spill detection algorithms using hybrid similarity measures", *Proceedings of Advances in Signal Processing and Communication – SPC 2018* (2018).

45. K. Shahi, H.Z.M. Shafri and A. Hamedianfar, "Road condition assessment by OBIA and feature selection techniques using very high-resolution WorldView-2 imagery", *Geocarto Int*. **32(12),** 1389–1406 (2017). https://doi.org/10.1080/10106049.2016.1213888

46. H. Ren, S. Xiao and H. Zhou, "A chi-square distance-based similarity measure of single-valued neutrosophic set and applications", *Int. J. Comput. Commun. Control* **14(1),** 78–89 (2019). https://doi.org/10.15837/ijccc.2019.1.3430

47. H. Chauhan and B. Krishna Mohan, "Effectiveness of spectral similarity measures to develop precise crop spectra for hyperspectral data analysis", *ISPRS Ann. Photogramm. Remote Sens. Spatial Inf. Sci.* **II(8),** 83–90 (2014). https://doi.org/10.5194/isprsannals-II-8-83-2014

48. C.-I. Chang, "Spectral information divergence for hyperspectral image analysis", *IEEE 1999 International Geoscience and Remote Sensing Symposium. IGARSS'99* (Cat. No.99CH36293), Hamburg, Germany, Vol. 1, pp. 509–511 (1999). https://doi.org/10.1109/IGARSS.1999.773549

49. N. Puletti, N. Camarretta and P. Corona, "Evaluating EO1-Hyperion capability for mapping conifer and broadleaved forests", *Eur. J. Remote Sens.* **49(1),** 157–169 (2016). https://doi.org/10.5721/EuJRS20164909

50. J.S. Pearlman, P.S. Barry, C.C. Segal, J. Shepanski, D. Beiso and S.L. Carman, "Hyperion, a space-based imaging spectrometer", *IEEE Trans. Geosci. Remote Sens.* **41(6),** 1160–1173 (2003). https://doi.org/10.1109/TGRS.2003.815018

51. R. Beck, *EO-1 User Guide v. 2.3*. University of Cincinnati (2003). http://www.pancroma.com/downloads/EO1userguidev2pt320030715UC.pdf

52. Y. Lu, Q. Tian, X. Wang, G. Zheng and X. Li, "Determining oil slick thickness using hyperspectral remote sensing in the Bohai Sea of China", *Int. J. Digit. Earth* **6(1),** 76-93 (2013). https://doi.org/10.1080/17538947.2012.695404

53. R.N. Adep, A. Shetty and H. Ramesh, "EXhype: A tool for mineral classification using hyperspectral data", *ISPRS J. Photogramm. Remote Sens.* **124,** 106–118 (2017). https://doi.org/10.1016/j.isprsjprs.2016.12.012

54. Research Systems, Inc., *FLAASH Module User's Guide*, ENVI FLAASH Version 4.2 (2005). http://www.spweather.com/enviuser/tutorial/misc/flaash.pdf

55. Y.C. Lu, W.X. Fu, Q.J. Tian, C.G. Lyu and W.C. Han, "Using optical remote sensing model to estimate oil slick thickness based on satellite image", *IOP Conf. Ser.: Earth Environ. Sci.* **17,** 012122 (2014). https://doi.org/10.1088/1755-1315/17/1/012122

56. J.H. Lumme, "Classification of vegetation and soil using imaging spectrometer data", *Geoscience and Remote Sensing Symposium* 83 (2004). https://www.isprs.org/proceedings/XXXV/congress/comm7/papers/16.pdf

57. A.J. Brown, "Spectral bluing induced by small particles under the Mie and Rayleigh regimes", *Icarus* 239, 85–95 (2014). https://doi.org/10.1016/j.icarus.2014.05.042

58. C.I. Chang, "An information-theoretic approach to spectral variability, similarity, and discrimination for hyperspectral image analysis", *IEEE Trans. Inform. Theory* **46(5),** 1927–1932 (2000). https://doi.org/10.1109/18.857802

59. R.N. Adep, A.P. Vijayan, A. Shetty and H. Ramesh, "Performance evaluation of hyperspectral classification algorithms on AVIRIS mineral data", *Pers. Sci.* **8,** 722–726 (2016). https://doi.org/10.1016/j.pisc.2016.06.070

60. Y. Du, C.-I. Chang, H. Ren, C.-C. Chang, J.O. Jensen and F.M. D'Amico, "New hyperspectral discrimination measure for spectral characterization", *Opt. Eng.* **43(8),** 1777–1786 (2004). https://doi.org/10.1117/1.1766301